SICE Journal of Control, Measurement, and System Integration, Vol. 11, No. 2, pp. 128–135, March 2018

A Three-Dimensional Skin-Shape Reproduction Mechanism for Evaluating the Risk of Wounds When Using a Wearable Robot

Yuma SAKAI *, Yasuhiro AKIYAMA *, Yoji YAMADA *, and Shogo OKAMOTO *

Abstract: When using a wearable robot, the interaction force applied at the point of contact may cause skin injuries. Therefore, validating the safety of wearable robots becomes important for their practical application. One method for evaluating contact safety at the fixation area of a wearable robot is to reproduce the relative motion and interaction force that occur at the area on a dummy. However, humans have various shapes, and evaluation of various human skin shapes is required. This study aims to develop a three-dimensional skin-shape reproduction mechanism with which to validate the safety of wearable robots. To that end, we have developed a simulation consisting of a cable-reinforced membrane that estimates surface deformation to examine different dummy shapes. Comparisons between device and simulation shapes validated the process of reproducing human skin and the range of deformation and elasticity of the dummy.

Key Words: wearable robot, contact safety, skin shape.

Nomenclature

γ_{xy}	Shearing strain of a membrane
$(\varepsilon_x)_k$	Strain of k-th cables in the x direction
$\left(\varepsilon_y\right)_l$	Strain of l-th cables in the y direction
ε_x	Strain of a membrane in the x direction
ε_y	Strain of a membrane in the y direction
A	Sectional area of cables
A_{ij}	In-plane stiffness of a membrane
E	Young's modulus of cables
H	Mean curvature
K	Number of cables in the x direction
L	Number of cables in the y direction
p	Inner pressure
T_{kx}	Tension of k-th cables in the x direction
T_{ly}	Tension of l-th cables in the y direction
u_k	Displacement in the x direction of k-th cables in the x direction
V_c	Strain energy of cables
v_l	Displacement in the y direction of l-th cables in the y direction
V_m	Strain energy of a membrane
W	External work
w	Displacement in the z direction
w_{kx}	Displacement in the z direction of k-th cables in the x direction
w_{ly}	Displacement in the z direction of l-th cables in the y direction

* Department of Mechanical Science and Engineering, Nagoya University, Furo-cho, Nagoya, Aichi 464-8603, Japan
E-mail: sakai.yuma@c.mbox.nagoya-u.ac.jp
(Received June 22, 2017)
(Revised October 3, 2017)

1. Introduction

The importance of wearable robots is increasing in aging societies, as such robots are expected to improve workforce productivity and quality of life for people with disabilities [1]–[3]. Thus, the use of these robots has begun to spread from hospitals and the rehabilitation field to society at-large. Whether for daily life or industry, the use of wearable robots is likely to expand.

Wearable robots are attached closely to the human body and exert assistive torque and force through the area at which fixation occurs [4]–[6]; hence, the safety of wearable robots should be considered carefully. For example, some studies have assessed conduction risks from wearable robots [7],[8] and examined human-robot interaction at the fixation area [9]–[11]. Further, the international standard ISO-13482:2014 [12] requires considering the contact safety of wearable robots.

Previously, our group developed a method with which to evaluate the contact safety of a wearable robot by estimating the risk of skin injury. For obvious ethical reasons, safety tests cannot endanger humans; therefore, we adopted a dummy to evaluate the risk of skin injury. For our dummy, we utilized porcine skin, which is a common substitute for human skin [13],[14] because of its proven durability against repetitive shear force [15] and similarity to human skin [16],[17]. To identify whether skin injury occurs when using a wearable robot, we observed the relative motion and interaction force applied by a robotic cuff during use [18],[19] and reproduced them using manipulator on the dummy skin [20],[21]. An overview of this safety evaluation test is shown in Fig. 1.

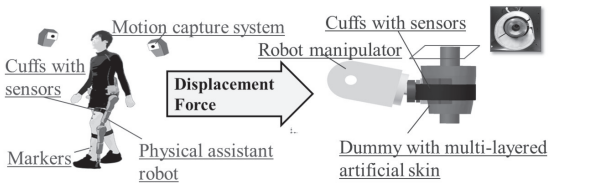

Compare the result with the conditions in which wounds occur (stress, amount of rubbing)

Fig. 1 The wounds risk evaluation process.

Fig. 2 An example human shape (pelvis).

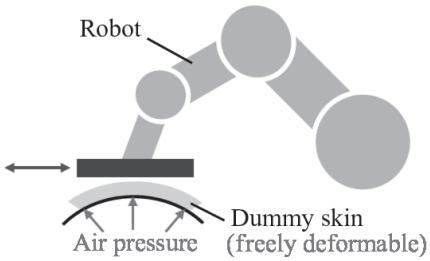

Fig. 3 Safety test with variable-shape dummy.

It would be reasonable to determine the representative human shape and evaluate the wounds risk of that shape. However, stress concentration, which affects wound risk, is probably caused by the unevenness of human shape as shown in Fig. 2 and their relationship has not been quantified. Thus, it is difficult to determine a typical human form to represent the risk of wounds to the user of a wearable device. In addition, actual wounds risk likely varies considerably because of individual differences in people's shapes [22]. Therefore, a transformable device that can mimic the variable features of human shape is required to evaluate the wound risk of wearable devices and analyze the stress concentration caused by surface unevenness.

Several methods for reproducing a 3D shape have previously been reported [23],[24]. A general method uses many pins equipped under each surface element; the surface shape is controlled by changing the height of each pin, arranged in a grid. However, this method requires that an actuator be equipped under each deformation area. The performance required of the device in this study is the control of shape and elasticity to emulate subsurface tissue. Hence, we employ a method that uses cables and air pressure, which can easily control shape and elasticity with only a few control parameters (the tension of each cable and air pressure).

Figure 3 depicts a safety validation test using a new device, in which a largely deformable membrane is manipulated using numerical pressure. In this study, we demonstrate the capacity

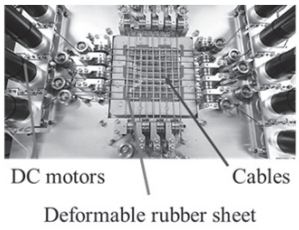

(a) Upper part of the shape-reproduction mechanism

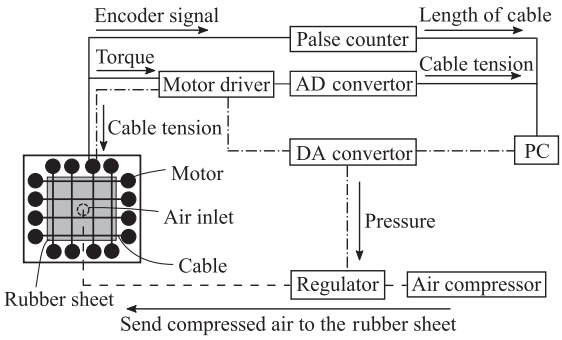

(b) Wiring diagram of the developed apparatus

Fig. 4 A 3D skin-shape reproduction mechanism.

of this device and the corresponding processes to reproduce a desired shape.

2. Development of a Three-Dimensional (3D) Skin-Shape Reproduction Mechanism

2.1 Surface Deformation Mechanism

The 3D shape-reproduction mechanism consists of DC motors (RE30, Maxon Motor, Switzerland), cables, and a silicon rubber sheet, as shown in Fig. 4 (a). The tension in each cable is controlled individually by a corresponding motor. The rubber sheet is inflated using air pressure injected from the bottom of the deformation area. Shape reproduction with the developed mechanism proceeds as follows: First, the deformable rubber sheet is pressurized and inflated. Then, the rubber sheet is restricted by adding tension to each cable. Because the tension of each cable can be set to a different value, a variety of deformation patterns, including different curvatures and local and asymmetric deformation, can be achieved.

2.2 Deformation Controller

A wiring diagram of the developed device is shown in Fig. 4 (b). The desired tension of each cable is input into motor drivers (ESCON 50/5, Maxon Motor, Switzerland) as the target torque of each motor. The drivers control corresponding motors using a PID algorithm. The actual motor torque is sent back to a computer monitoring actual condition. The air pressure of the rubber sheet is controlled by a regulator (ITV-1010312S, SMC Corporation, Japan) in the same manner as the motor torque.

2.3 Deformation Ability of the Developed Device

2.3.1 Basic conditions

The developed mechanism was used to reproduce shapes. The physical parameters, geometry, and experimental conditions of the device are shown in Fig. 5 and Table 1 with air pressure p and cable tensions T_{kx} and T_{ly} as input parameters. The

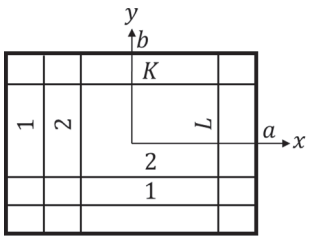

Fig. 5 Cable-restricted membrane [25].

Table 1 Conditions of shape reproduction.

Air pressure p	0.02 MPa
Young's modulus (Rubber sheet)	8.9 MPa
Young's modulus (Cable) E	70.5 GPa
Poisson's ratio (Rubber sheet)	0.5
Thickness of rubber sheet	2.0 mm
Deformation area (x-direction)	90 mm
Deformation area (y-direction)	90 mm
Number of cables (x-direction) K	9
Number of cables (y-direction) L	9
Initial tension of cables T_{kx}, T_{ly}	1.0 N

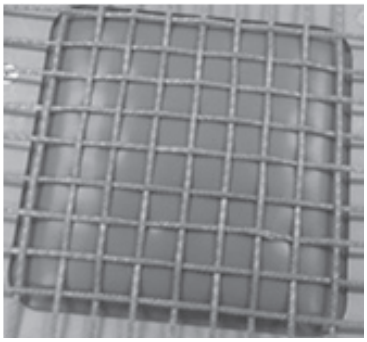

Fig. 6 The result of shape reproduction.

other conditions reflect the mechanical parameters of the developed mechanism. The deformed shape is shown in Fig. 6. Owing to the restriction of the deformation applied by the cables, the inflation of the center of the rubber sheet is especially restricted. Additionally, the developed mechanism must support the dummy skin during wound risk evaluation. Therefore, the deformable rubber sheet was more rigid than muscle [26]–[28].

2.3.2 Shape with large local deformation

Because of the unevenness of actual human skin, which includes local convexities, large deformations should be considered. Thus, to reproduce large local deformations, cable tensions were adjusted separately. Air pressure was set to 0.1 MPa and the cable tensions were 0 N in the deformed area (k = 4, 5, 6, l = 4, 5, 6) and 10 N elsewhere. The shape reproduced using the new conditions is shown in Fig. 7, in which it can be observed that only the central area of the rubber is significantly deformed.

We then compared the displacements and mean curvature of the rubber sheet in cross-section in the two conditions, calculating the displacement and curvature at every center point of the wire grid in the x-direction. We employed a 3D scanner (Artec Space Spider, Artec 3D, Luxembourg) to measure the shape of the deformed surface. The mean curvature is the arithmetic mean of the principal curvatures at points in the region. Curvature can be calculated as follows:

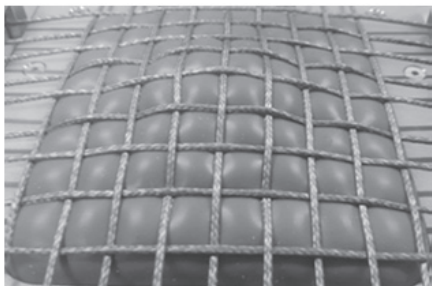

Fig. 7 Reproduction of a shape with a large local deformation.

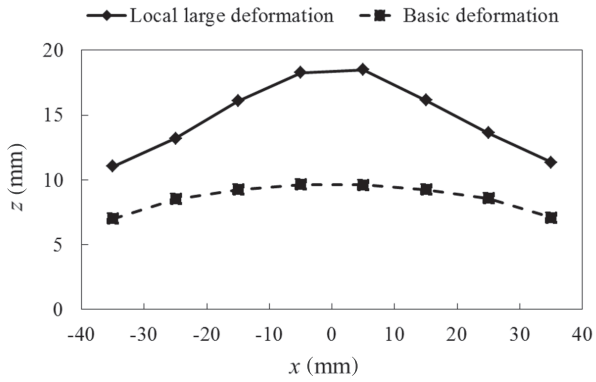

(a) Displacement comparison

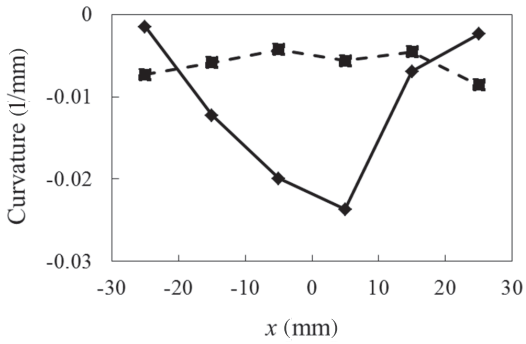

(b) Curvature comparison

Fig. 8 Numerical analysis of a reproduced shape with a large local deformation.

$$H = \frac{1}{2\left\{1 + (\partial_x w)^2 + \left(\partial_y w\right)^2\right\}^{\frac{3}{2}}}\left[\partial_{xx} w\left\{1 + \left(\partial_y w\right)^2\right\}\right.$$

$$\left. -2\partial_x w \partial_y w \partial_{xy} w + \partial_{yy} w\left\{1 + (\partial_x w)^2\right\}\right]. \quad (1)$$

This study emphasized the reproduction of curvatures, because the risk of wounds is probably related to curvature. The shear stress that occurs between a robotic cuff and human skin increases in areas of high curvature because of its concentration. Thus, wound risk possibly increases in such areas.

The comparison between displacement and curvature is shown in Fig. 8. In this figure, the curvature is negative when the displacement is convex. From these results, we can confirm our mechanism's ability to reproduce large local deformations.

2.3.3 Asymmetric shape

Similarly, we conducted an experiment to confirm the reproducibility of asymmetric shapes. For asymmetric deformation, the air pressure was set to 0.05 MPa and the cable tensions were 10 N in the strongly restricted area (k = 1, 2, 3) and 0 N else-

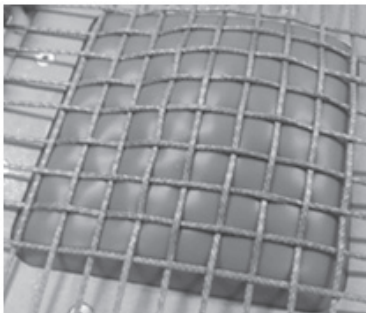

Fig. 9 Reproduction of an asymmetric shape.

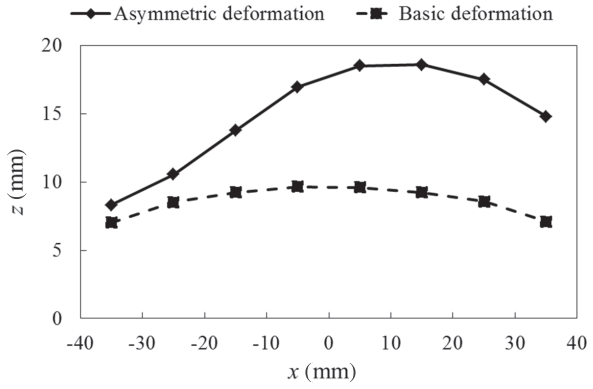

(a) Displacement comparison (asymmetric shape)

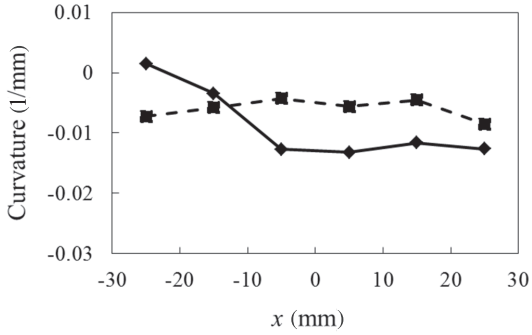

(b) Curvature comparison (asymmetric shape)

Fig. 10 The result of an asymmetric shape reproduction.

where. The asymmetric conditions, in which only the right side of the rubber area is deformed, are shown in Fig. 9. We found the displacements and mean curvatures to be similar to those of the shape with a large local deformation, as shown in Fig. 10. Given these results, we could confirm the reproducibility of asymmetric shapes.

2.4 Mechanical Properties of Reproducing Shapes

The deformed surface is comprised of a rigid base and elastic tissue that mimic the musculoskeletal system, as well as a covering surface that mimics skin or soft tissue. That is, the deformed shape must reproduce the mechanical properties of human bone, muscle, and fat. Therefore, in this study, we measured the elasticity of the deformed surface using a device consisting of a linear slider, contactor, and load cell. The linear slider was fixed vertically from the fixed flame. Then, the load cell and contactor were also fixed on the slider. The compression force applied to the contactor was measured by the load cell. The device used for the elasticity measurement is shown

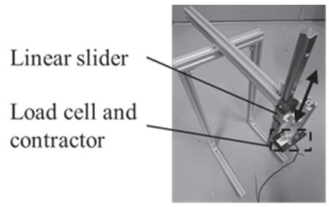

Load cell and contractor moves in the vertical direction along the linear slider

Fig. 11 Device for the elasticity measurement.

in Fig. 11. The pressure was set to 0.1 MPa and the maximum stroke of the contactor was 5 mm. The stress per displacement was thus measured as 102 kPa/mm. The pressure applied to the cuff can be calculated experimentally by recording the interaction force applied when using a wearable robot [15]. Because the pressure (9.38 kPa) corresponded to a displacement of 0.09 mm considering the elasticity of the deformed surface, the deformation of the rubber sheet can be ignored when the reproduced motion and force are applied to the device in safety tests. Thus, we confirm that the device is sufficiently rigid to model human musculoskeletal tissue. On the other hand, the rigidity of relaxed muscle with a large deformation can be calculated as approximately 5.5 kPa/mm from the strain-stress diagram [29]. Although the rigidity observed in the device was too high, the elasticity of the deformed area can be modified by changing the pressure or adding a softer surface sheet.

3. Deformation Estimation of Cable-Restricted Membrane

When conducting shape reproduction, the cable tension and air pressure, which reproduce the objective shape, should be related to the surface shape to control the surface shape freely. Therefore, deformation simulation is required to determine the value of such input parameters.

3.1 Fundamental Equations of the Deformation Analysis

In this simulation, we assumed that the cables touched the membrane constantly. In addition, for simplicity, the initial deflection, bending stiffness, friction coefficient, and volume of the cable were ignored. Strain-displacement relations of the cable-restricted membrane are shown in the following equations [30].

$$\begin{cases} \varepsilon_x = \dfrac{\partial u}{\partial x} + \dfrac{1}{2}\left(\dfrac{\partial w}{\partial x}\right)^2, \\ \varepsilon_y = \dfrac{\partial v}{\partial y} + \dfrac{1}{2}\left(\dfrac{\partial w}{\partial y}\right)^2, \\ \gamma_{xy} = \dfrac{\partial u}{\partial y} + \dfrac{\partial v}{\partial x} + \dfrac{\partial w}{\partial x}\dfrac{\partial w}{\partial y}. \end{cases} \tag{2}$$

Further, the strain-displacement relations of the cables in the x- and y-axes are

$$\begin{cases} (\varepsilon_x)_k = \dfrac{\partial u_k}{\partial x} + \dfrac{1}{2}\left(\dfrac{\partial w_{kx}}{\partial x}\right)^2, \\ \left(\varepsilon_y\right)_l = \dfrac{\partial v_l}{\partial y} + \dfrac{1}{2}\left(\dfrac{\partial w_{ly}}{\partial y}\right)^2. \end{cases} \tag{3}$$

Moreover, the potential energy Π of the cable-restricted membrane is shown in the following equation [25],[30]:

$$\Pi = V_m + V_c - W, \tag{4}$$

where V_m, and V_c are as follows:

$$V_m = \frac{1}{2}\iint \left(A_{11}{\varepsilon_x}^2 + A_{22}{\varepsilon_y}^2 + A_{66}{\gamma_{xy}}^2 + 2A_{12}\varepsilon_x\varepsilon_y + 2A_{16}\varepsilon_x\gamma_{xy} + 2A_{26}\varepsilon_y\gamma_{xy}\right)dxdy, \tag{5}$$

$$V_c = \frac{1}{2}\sum_{k=1}^{K}\int\left[EA\left\{(\varepsilon_x)_k\right\}^2 + T_{kx}\left(\frac{\partial w_{kx}}{\partial x}\right)^2\right]dx, + \sum_{l=1}^{L}\int\left[EA\left\{\left(\varepsilon_y\right)_l\right\}^2 + T_{ly}\left(\frac{\partial w_{ly}}{\partial y}\right)^2\right]dy, \tag{6}$$

$$W = p\iint w dxdy. \tag{7}$$

Next, the boundary conditions of the rectangle membrane to which the edge of the membrane is fixed are

$$\begin{cases} x = \pm a : u = v = w = 0, \\ y = \pm b : u = v = w = 0, \end{cases} \tag{8}$$

and the displacement functions of the membrane, which fulfill the boundary conditions, are assumed to be as follows [25]:

$$\begin{cases} u(x,y) = \displaystyle\sum_{m=1}^{M}\sum_{n=1}^{N} U_{mn}\sin\frac{m\pi}{2a}(x+a)\sin\frac{n\pi}{2b}(y+b), \\ v(x,y) = \displaystyle\sum_{m=1}^{M}\sum_{n=1}^{N} V_{mn}\sin\frac{m\pi}{2a}(x+a)\sin\frac{n\pi}{2b}(y+b), \\ w(x,y) = \displaystyle\sum_{m=1}^{M}\sum_{n=1}^{N} W_{mn}\sin\frac{m\pi}{2a}(x+a)\sin\frac{n\pi}{2b}(y+b). \end{cases} \tag{9}$$

Similarly, the displacement functions of the cable that fulfill the boundary conditions are assumed as follows [25]:

$$\begin{cases} u_k(x) = \displaystyle\sum_{m=1}^{M}\sum_{n=1}^{N} U_{mn}\sin\frac{m\pi}{2a}(x+a)\sin\frac{n\pi k}{K+1}, \\ w_{kx}(x) = \displaystyle\sum_{m=1}^{M}\sum_{n=1}^{N} W_{mn}\sin\frac{m\pi}{2a}(x+a)\sin\frac{n\pi k}{K+1}, \end{cases} \tag{10}$$

$$\begin{cases} v_l(y) = \displaystyle\sum_{m=1}^{M}\sum_{n=1}^{N} V_{mn}\sin\frac{m\pi l}{L+1}\sin\frac{n\pi}{2b}(y+b), \\ w_{ly}(y) = \displaystyle\sum_{m=1}^{M}\sum_{n=1}^{N} W_{mn}\sin\frac{m\pi l}{L+1}\sin\frac{n\pi}{2b}(y+b). \end{cases} \tag{11}$$

By substituting strain-displacement relations (Eqs. (2) and (3)) and displacement functions (Eqs. (9), (10), and (11)) into Eq. (4), we can express the potential energy using the unknown constants U_{mn}, V_{mn}, and W_{mn}. We can obtain the unknown constants by minimizing potential energy [25]. In this study, the deformation of the cable-restricted membrane is obtained by determining the unknown coefficients that minimize the potential energy at the specified air pressure. Therefore, the optimization problem is defined as follows:

$$\min \quad J = \Pi \tag{12}$$

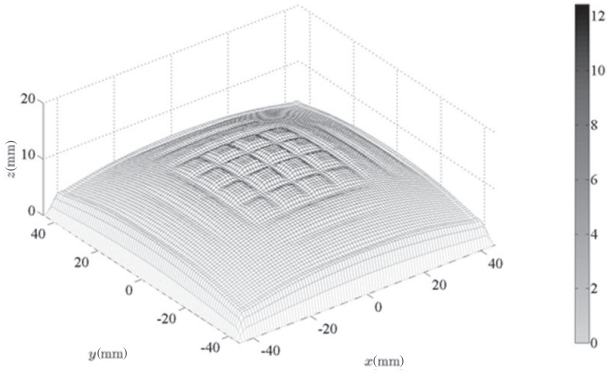

Fig. 12 Deformation analysis of the cable-restricted membrane.

where J is the objective function having U_{mn}, V_{mn}, and W_{mn} as decision variables. The Broyden-Fletcher-Goldfarb-Shanno (BFGS) algorithm, which is a quasi-Newtonian method, was used for optimization [25].

3.2 Deformation Analysis of the Cable-Restricted Membrane

The result of the deformation simulation is shown in Fig. 12. In this simulation, the condition was the same as in Table 1, except for a Young's modulus of 1.5 GPa. The difference occurred because a nylon cable, which was originally used in the device, was assumed in this simulation. As the boundary condition, displacement at the edge of the deformable area was set to 0.

4. Validity Evaluation of the Deformation Analysis

The deformed shape was compared between the simulation and device to evaluate the performance and feasibility of using simulation to obtain the input value of the device from surface shape. The same input parameters (cable tension and air pressure) were used for each method.

4.1 Appearance Comparison

The shape reproduced with the 3D deformation device is shown in Fig. 13. As mentioned above, a nylon cable was used in this experiment as same as the simulation. The effect of the cable restriction was observed only around the center of the rubber sheet, as shown in Figs. 12 and 13. This result corroborates the validity of the developed mechanism.

4.2 Displacement Comparison

For more detailed evaluation, we compared the displacement of cross-sections of both methods. The displacement in the z-axis of both methods was compared as in previous sections, the result of which is shown in Fig. 14 (a). This comparison suggests that, despite the small difference between the two methods (especially around the area slightly separated from the center of deformation), the difference is at most 0.7 mm, which is negligible when reproducing contact conditions between a wearable robot and its human wearer. Therefore, we can conclude that the shapes of the deformation simulation and the reproduced device shape matched at a level that would produce no practical problems.

4.3 Curvature Comparison

We similarly compared the mean curvatures of the two shapes at the center of the wire grid along the x-direction, which

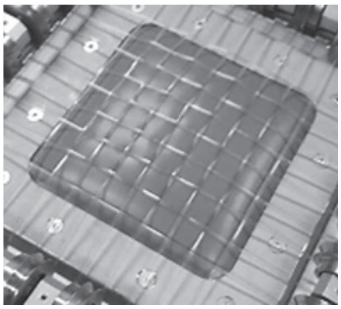

Fig. 13 Reproducing shape with the developed mechanism.

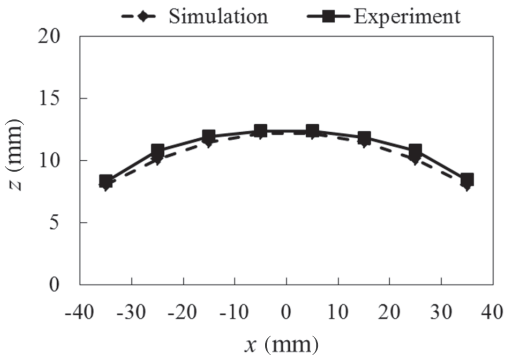

(a) Displacement comparison between experiment and simulation

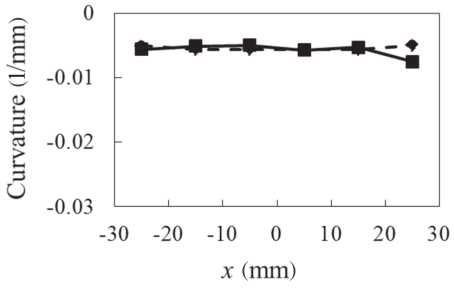

(b) Curvature comparison between experiment and simulation

Fig. 14 Displacement and curvature comparison between actual reproduced shape and result of deformation analysis.

is shown in Fig. 14 (b). In this result, the curvatures of the two shapes nearly match, suggesting at the validity of the simulation for the deformation of the cable-restricted membrane.

5. Discussion

The developed surface deformation mechanism and simulation are integrated into a 3D skin-shape reproduction system to improve the method by which we evaluate the contact safety of a wearable robot. In this system, shape reproduction is conducted as shown in Fig. 15. In this process, the optimization of the design parameters (air pressure and cable tensions) is included.

First, as shown in Fig. 2, the shape of the skin at the test area is measured or modeled. Then, using a deformation analysis that calculates the surface shape from the pressure and tension of each cable of the surface deformation mechanism, we can calculate the input parameters of the surface deformation device with an optimization process using sequential quadratic programming. Thus, an objective shape is reproduced by inputting the optimized parameters into the developed mechanism. Then,

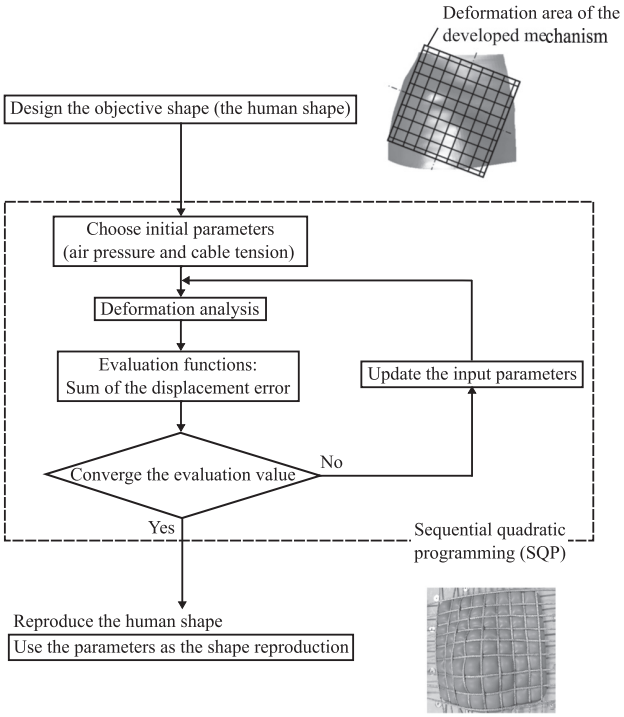

Fig. 15 The shape reproduction process.

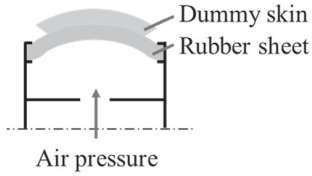

Fig. 16 Cross-section of the reproduced shape.

the dummy skin is put on the reproduced shape and wound risk evaluation can be conducted.

A cross-section of the reproduced shape during this process is shown in Fig. 16. The dummy skin, which covers the deformed surface, is used not only to diminish the unevenness of the surface, which comes from the inflation of the rubber sheet between cable restrictions, but also to modify the physical parameters of the skin surface. Although the device is capable of mimicking the rigidity of the musculoskeletal system, surface friction should be adjusted by using artificial skin. In addition, the unevenness in the rigidity of actual humans, which comes from differences in tissue thickness, should be adjusted.

As mentioned above, the proposed device has sufficient deformation ability to reproduce the shape of uneven skin of the human. In addition, the deformation, which reproduced a basic shape, of the device and simulation matched. Although the simulation should be improved to reproduce larger deformation and the shape reproduction system should be installed, the feasibility of the skin-shape reproduction process is demonstrated in this paper.

In this study, we only focused on the effect of parts where the wounds risk becomes particularly large, which is reflected in our reproductions. However, if required for evaluating wound risks, we can adopt a wider reproduction area that consists of components with different physical coefficients by combining smaller sections.

6. Conclusion

In this study, we developed a 3D skin-shape reproduction mechanism for use in evaluating the risk of skin injury around the fixation point of a wearable robot. We confirmed the ability of this mechanism to reproduce the convexity and curvature of human skin. In addition, we have made suggestions for the possibility of adjusting the rigidity of the surface to that of various human tissue. Then, to control the surface shape, we developed a simulator that estimates the surface shape from the input parameters of the device (the pressure and tension of each cable). The similarity in surface shape between the simulation and device suggest the simulation's validity. Furthermore, we introduced and optimized a flow with which to reproduce a desired shape and physical parameters corresponding to human characteristics. Thus, in this study, we have proposed a method that can consider human individuality in determining the risk of skin injury and evaluated its validity. By using this method, the evaluation of the wound risk can be conducted in made to order. This method helps not only to evaluate the risk of skin injury of individuals but also to analyze the relationships between the risk of skin injury and cuff motion, skin shape, and physical parameters, which are important for improving the contact safety of wearable robots.

Acknowledgments

This study is based on the results of research and development of Japan Agency for Medical Research and Development (Project to Promote the Development and Introduction of Robotic Devices for Nursing Care).

References

[1] H.S. Lo and S.Q. Xie: Exoskeleton robots for upper-limb rehabilitation: State of the art and future prospects, *Medical Engineering & Physics*, Vol. 34, No. 3, pp. 261–268, 2012.

[2] S. Mohammed, Y. Amirat, and H. Rifai: Lower-limb movement assistance through wearable robots: State of the art and challenges, *Advanced Robotics*, Vol. 26, No. 1-2, pp. 1–22, 2012.

[3] K. Kong and D. Jeon: Design and control of an exoskeleton for the elderly and patients, *IEEE/ASME Transactions on Mechatronics*, Vol. 11, No. 4, pp. 428–432, 2006.

[4] E. Rocon, J.M. Belda-Lois, A.F. Ruiz, M. Manto, J.C. Moreno, and J.L. Pons: Design and validation of a rehabilitation robotic exoskeleton for tremor assessment and suppression, *IEEE Transactions on Neural Systems and Rehabilitation Engineering*, Vol. 15, No. 3, pp. 367–378, 2007.

[5] K. Suzuki, G. Mito, H. Kawamoto, Y. Hasegawa, and Y. Sankai: Intention-based walking support for paraplegia patients with robot suit HAL, *Advanced Robotics*, Vol. 21, No. 12, pp. 1441–1469, 2007.

[6] H. In, B.B. Kang, M.K. Sin, and K.-J. Cho: Exo-glove: A wearable robot for the hand with a soft tendon routing system, *IEEE Robotics & Automation Magazine*, Vol. 22, No. 1, pp. 97–105, 2015.

[7] C. Nabeshima, H. Kawamoto, and Y. Sankai: Typical risks and protective measures of wearable walking assistant robots, *2011 IEEE/SICE International Symposium on System Integration (SII)*, pp. 914–919, 2011.

[8] C. Nabeshima, H. Kawamoto, and Y. Sankai: Strength testing machines for wearable walking assistant robots based on risk assessment of robot suit HAL, *2012 IEEE International Conference on Robotics and Automation (ICRA)*, pp. 2743–2748, 2012.

[9] Y. Akiyama, Y. Yamada, K. Ito, S. Oda, S. Okamoto, and S. Hara: Test method for contact safety assessment of a wearable robot-analysis of load caused by a misalignment of the knee joint, *2012 IEEE RO-MAN*, pp. 539–544, 2012.

[10] T. Lenzi, N. Vitiello, S.M.M.D. Rossi, A. Persichetti, F. Giovacchini, S. Roccella, F. Vecchi, and M.C. Carrozza: Measuring human–robot interaction on wearable robots: A distributed approach, *Mechatronics*, Vol. 21, No. 6, pp. 1123–1131, 2011.

[11] R. Alami, A. Albu-Schäffer, A. Bicchi, R. Bischoff, R. Chatila, A.D. Luca, A.D. Santis, G. Giralt, J. Guiochet, G. Hirzinger, et al.: Safe and dependable physical human-robot interaction in anthropic domains: State of the art and challenges, *2006 IEEE/RSJ International Conference on Intelligent Robots and Systems*, pp. 1–16, 2006.

[12] International Standards Organization (ISO): Robots and Robotic Devices - Safety Requirements for Personal Care Robots, No. ISO 13482, Geneva: ISO, 2014.

[13] W. Meyer: Comments on the suitability of swine skin as a biological model for human skin, *Der Hautarzt; Zeitschrift fur Dermatologie, Venerologie, und verwandte Gebiete*, Vol. 47, No. 3, pp. 178–182, 1996 (German).

[14] M. Swindle: Porcine integumentary system models: part 1-dermal toxicology, Sinclair Research Centre, 2008.

[15] X. Mao, Y. Yamada, Y. Akiyama, S. Okamoto, and K. Yoshida: Safety verification method for preventing friction blisters during utilization of physical assistant robots, *Advanced Robotics*, Vol. 31, No. 13, pp. 680–694, 2017.

[16] P.F.D. Naylor: The skin surface and friction, *British Journal of Dermatology*, Vol. 67, No. 7, pp. 239–246, July 1955.

[17] P.F.D. Naylor: Experimental friction blisters, *British Journal of Dermatology*, Vol. 67, No. 10, pp. 327–342, 1955.

[18] Y. Akiyama, S. Okamoto, Y. Yamada, and K. Ishiguro: Measurement of contact behavior including slippage of cuff when using wearable physical assistant robot, *IEEE Transactions on Neural Systems and Rehabilitation Engineering*, Vol. 24, No. 7, pp. 784–793, 2016.

[19] Y. Akiyama, Y. Yamada, and S. Okamoto: Interaction forces beneath cuffs of physical assistant robots and their motion-based estimation, *Advanced Robotics*, Vol. 29, No. 20, pp. 1315–1329, 2015.

[20] K. Yoshida, Y. Yamada, Y. Akiyama, S. Hara, and S. Okamoto: Development of a safety validation test equipment for severity estimation of wounds caused by physical assistant robot, *Proceedings of the RSJ/SICE/JSME 20th Robotics Symposia*, Karuizawa, Nagano, Japan, pp. 483–488, 2015 (Japanese).

[21] X. Mao, Y. Yamada, Y. Akiyama, S. Okamoto, and K. Yoshida: Development of a novel test method for skin safety verification of physical assistant robots, *2015 IEEE International Conference on Rehabilitation Robotics (ICORR)*, pp. 319–324, 2015.

[22] Z.B. Azouz, M. Rioux, C. Shu, and R. Lepage: Analysis of human shape variation using volumetric techniques, *Proc. International Conference on Computer Animation and Social Agents*, pp. 197–206, 2004.

[23] H. Iwata, H. Yano, F. Nakaizumi, and R. Kawamura: Project FEELEX: Adding haptic surface to graphics, *Proceedings of the 28th Annual Conference on Computer Graphics and Interactive Techniques*, pp. 469–476, ACM, 2001.

[24] M. Nakatani, H. Kajimoto, K. Vlack, D. Sekiguchi, N. Kawakami, and S. Tachi: Control method for a 3D form display with coil-type shape memory alloy, *Proceedings of the 2005 IEEE International Conference on Robotics and Automation, 2005, ICRA 2005*, pp. 1332–1337, 2005.

[25] H. Sekine, H. Fukunaga, and N. Saitou: Noniinear deformation analysis of air-dome membrane structures, *Transactions of the Japan Society of Mechanical Engineers*, Vol. 63, No. 605, pp. 117–123, 1997 (in Japanese).

[26] A. Nordez and F. Hug: Muscle shear elastic modulus measured

using supersonic shear imaging is highly related to muscle activity level, *Journal of Applied Physiology*, Vol. 108, No. 5, pp. 1389–1394, 2010.
[27] B.C.W. Kot, Z.J. Zhang, A.W.C. Lee, V.Y.F. Leung, and S.N. Fu: Elastic modulus of muscle and tendon with shear wave ultrasound elastography: Variations with different technical settings, *PloS One*, Vol. 7, No. 8, e44348, 2012.
[28] K. Chino, R. Akagi, M. Dohi, S. Fukashiro, and H. Takahashi: Reliability and validity of quantifying absolute muscle hardness using ultrasound elastography, *PLoS One*, Vol. 7, No. 9, e45764, 2012.
[29] K. Isogai, S. Okamoto, Y. Yamada, R. Ayabe, and K. Ohtawa: Skin-fat-muscle urethane model for palpation for muscle disorders, *2015 IEEE/SICE International Symposium on System Integration (SII)*, pp. 960–964, 2015.
[30] G.C. Tsiatas and J.T. Katsikadelis: Large deflection analysis of elastic space membranes, *International Journal for Numerical Methods in Engineering*, Vol. 65, No. 2, pp. 264–294, 2006.

Yuma Sakai

He received the B.E. degree in engineering from Nagoya University, Nagoya, Japan, in 2016. He is currently a master's course student at Nagoya University. His research interests are human-robot interaction, wearable robotics, and mechanical safety.

Yasuhiro Akiyama

He received the B.E. degree in engineering from Tokyo Institute of Technology, Tokyo, Japan, in 2006, and the M.S. and the Ph.D. degrees in engineering from the University of Tokyo, Tokyo, Japan, in 2008 and 2011, respectively. Since 2016, he has been an assistant professor at the Graduate School of Engineering, Nagoya University. His main areas of research interests are mechanical safety, human-robot interaction, and manned space mission.

Yoji Yamada (Member)

He received a doctor degree from Tokyo Institute of Technology in 1990. He had been with Toyota Technological Institute since 1983 and became an associate professor in the Graduate School of the Institute. In 2004, he joined Intelligent Systems Research Institute of National Institute of Advanced Industrial and Science Technology (AIST). In 2009, he moved to the Department of Mechanical Science and Engineering, Graduate School of Engineering, Nagoya University as a professor. His current research interests include safety and intelligence technology in human/machine systems, their robotic sensing and control.

Shogo Okamoto

He received M.S. and Ph.D. degrees in information sciences in 2007 and 2010, respectively, from the Graduate School of Information Sciences, Tohoku University. Since 2016, he has been a senior lecturer at the Graduate School of Engineering, Nagoya University. His research interests include haptics and human-assistive technology.